DOI: ADD DOINUMBER HERE

# Improving PIC-DSMC Simulations of RF Plasmas via Event Splitting

*Oblapenko Georgii*[1], *Goldstein David*[2], *Varghese Philip*[2,3], *and Moore Christopher*[4]
[1] *German Aerospace Center (DLR)*
*Bunsenstrasse 10, 37073 Göttingen, Germany*
georgii.oblapenko@dlr.de
[2] *ASE-EM Department, The University of Texas at Austin*
*2617 Wichita St., Stop C0600, Austin, TX 78712*
david@oden.utexas.edu
[3] *Oden Institute for Computational Engineering and Sciences, The University of Texas at Austin*
*2201 E 24th St, StopC0200, Austin, TX 78712*
varghese@mail.utexas.edu
[4] *Sandia National Laboratories*
*Albuquerque, NM, USA,*
chmoore@sandia.gov

## Abstract

Particle-in-Cell Direct Simulation Monte Carlo (PIC-DSMC) is a widely used method for simulation of non-equilibrium plasmas, especially when the plasma flow is rarefied, and the applicability of fluid models is questionable. However, the PIC-DSMC method is subject to stochastic noise, and depending on the process being simulated, might require extremely large computational efforts. Therefore, the improvement of accuracy of PIC-DSMC methods is a topic of active research. In the present work, a recently developed collision and boundary condition treatment scheme, dubbed "event splitting", which aims at improving simulation of low-probability processes, is applied to ionization processes in xenon and helium plasmas, where it shown to reduce the level of stochastic noise compared to standard DSMC collision schemes.

## 1. Introduction

The rarefied nature of plasma flows in a variety of applications, including electric propulsion, precludes the use of fluid-based models for their simulation.[4,11,26] The wide range of densities of the constituent species in such flows necessitates the use of variable-weight particles.[2,23] As such, the flow simulations are complicated not only due to the stochastic nature of the PIC-DSMC method, but also due to the particle splitting during collisions and the subsequent particle merging required.[3,12–14] Moreover, PIC-DSMC simulations can be sensitive to the number of particles used in the simulation, choice of movement integration scheme, and timestep choice.[17,27]

In electric propulsion modelling, the need to model low-probability events accurately is highly relevant to different aspects of the thruster design, including the impact of charge-exchange (CEX) collisions on gridded thruster erosion and surface contamination,[2,5,11,18] the influence of gas-surface interactions on air-breathing thruster inlet design,[24] and the role of electron-impact ionization and excitation reactions on instabilities in Hall thrusters.[7–9]

Recently, an extension of the Stochastic Weighted Particle Method (SWPM)[23] to multi-species flows was proposed,[2] and the impact of the choice of collision multiplier on the accuracy of ion flux simulation was studied. The use of a collision multiplier allows one to perform more collisions per timestep by splitting the particles involved in the collisions, thus increasing the chance that the colliding particles will undergo a low-probability process. In the referenced work it was shown that the use of collision multipliers for CEX collisions allows one to reduce the particle count and simulation runtime by an order of magnitude, whilst retaining the same accuracy in the ion flux compared to a simulation using a very large number of particles and no collision multipliers.

Another approach to improvement of modelling of low-probability processes was recently proposed,[19,20] dubbed "event splitting", in which the variable-weight particles are split proportionally to the probabilities of processes that can take place during a given collision. It was shown that use of event splitting for collisions and boundary conditions with secondary emission can noticeably reduce the noise in PIC-DSMC simulations compared to the use of standard sampling approaches to collision process modelling.

In the present work, the event splitting collision scheme is applied to spatially homogeneous xenon and helium plasmas, in order verify the results with the reference Bolsig+ solver[6] and compare the performance of two different variable-weight particle collision selection schemes: the variable-weight No Time Counter (NTC) scheme[25] and the multi-species Stochastic Weighted Particle Method scheme (SWPM).[2] The event splitting scheme is then applied to simulation of xenon and helium capacitively coupled RF plasmas and compared with the usual DSMC sampling procedure.

## 2. Variable Weight DSMC Collision Schemes

A brief overview of the collision schemes investigated in the present paper is presented. First, we consider the collision partner selection schemes. The variable-weight No Time Counter (NTC)[25] defines the number of $c$-$d$ collisions to be selected in a cell as:

$$N_{coll,cd} = \left\lfloor \frac{1}{V} N_{p,c} N_{p,d} (w\sigma_{tot} g)_{\max} \Delta t + \mathcal{R} \right\rfloor. \tag{1}$$

Here $V$ is the volume of the physical cell, $N_{p,c}$ and $N_{p,d}$ are the number of DSMC particles of species $c$ and $d$ respectively, $(w\sigma_{tot}g)_{\max}$ is the maximum value of $w \cdot \sigma_{tot} \cdot g$ in the physical cell, $g$ is the relative velocity of the colliding particles, $\sigma_{tot}(g)$ is the total collision cross-section, $w$ is the computational weight of the particles, and $\Delta t$ is the timestep. For the case of same-species collisions, the quantity $N_{p,c}N_{p,d}$ is replaced by $\frac{1}{2}N_{p,c}(N_{p,c} - 1)$. Finally, $\mathcal{R} \sim \mathcal{U}(0, 1)$ is a random number sampled from the uniform distribution over the interval $[0, 1]$.

$N_{coll}$ potential collision pairs are selected, and checked for collisions. Assuming that particles with weights $w_1$ and $w_2$ and a relative velocity $g$ were chosen the collision is accepted with a probability of

$$P = \frac{\mathrm{MAX}(w_1, w_2)\sigma_{tot} g}{(w\sigma_{tot} g)_{\max}}, \tag{2}$$

where the cross-section $\sigma_{tot}$ is computed for the pair in question.

In the SWPM multi-species scheme, the number of collisions is computed as

$$N_{coll,cd} = \left\lfloor \frac{1}{V} c_m N_{p,c} N_{p,d} \left(\overline{w_c} + \overline{w_d} - w_{min}\right) (\sigma_{tot} g)_{\max} \Delta t + \mathcal{R} \right\rfloor. \tag{3}$$

Here $w_{min}$ is the smallest weight of all particles of species $c$ and $d$ in the cell, and $\overline{w_c}$ and $\overline{w_d}$ are the average weights of particles of species $c$ and $d$ in the cell, respectively. $c_m$ is the aforementioned collision multiplier, which in the present work is taken to be equal to 1. After $N_{coll}$ is computed, the random collision pairs are selected, and first are accepted with a probability

$$P = \frac{w_1 + w_2 - w_{min}}{w_{max,c} + w_{max,d} - w_{min}}, \tag{4}$$

where $w_1$ and $w_2$ are the weights of the selected particles and $w_{max,c}$, $w_{max,d}$ are the maximum weights of particles of species $c$ and $d$ in the cell, respectively. Finally, if a pair is accepted, a collision occurs with a probability of

$$P = \frac{\mathrm{MAX}(w_1, w_2)(\sigma_{tot} g)}{(w_1 + w_2 - w_{min})(\sigma_{tot} g)_{\max}}. \tag{5}$$

Finally, in both the NTC and SWPM schemes, once a collision pair is selected and accepted, the particle with the larger computational weight (we assume without loss of generality that it is the particle with weight $w_1$) is split into two particles with weights $w_1 - w_2$ and $w_2$, and only the equal-weight particles with weights $w_2$ are collided. As mentioned in the introduction, this constant creation of particles during collisions requires the use of particle merging procedures in order to keep the particle counts bounded.[14]

Compared to the variable-weight NTC scheme, the SWPM scheme requires an additional step of acceptance-rejection, and keeping track of the minimum, maximum, and average particle weights in the cell. However, depending on the distribution of the particle weights in phase space, the schemes may perform differently in terms of computational efficiency, and therefore, both schemes are examined for the spatially homogeneous flow studies in the present work.

If during a collision of two particles $N_{proc}$ processes can occur (with associated probabilities $p_i$, $i = 1, \ldots, M_{proc}$), the standard DSMC approach is to sample a process to simulate according to the probabilities $p_i$; thus, processes (such as ionization reactions, internal energy transitions, etc.) with higher probabilities are simulated more frequently. In contrast, within the framework of the "event splitting" scheme,[19] the colliding particles (with weights $w_2$) are split further proportionally to the probabilities $p_i$. After the splitting, all of the newly created particles (with weights $w_2 p_i$, $i = 1, \ldots, M_{proc}$) undergo the corresponding collisional process $i$. Thus, for each collision, all possible processes are simulated simultaneously. As a result, one obtains a lower level of stochastic noise in the simulation of collisional processes, and as the probability of the process decreases, the advantage of the event splitting scheme over standard DSMC approach increases.

## 3. Numerical Results

### 3.1 0-D Ionization

We first consider a spatially homogeneous test case, in which a gas is seeded with a small fraction of electrons and ions, and the charged particles are accelerated by a constant electric field. As the electrons accelerate, they gain energy, which they subsequently lose due to collisions with the neutral species. After an initial transient period, the system reaches a steady state, characterized by a constant electron temperature and ionization rate coefficient. The values of the electron temperature and ionization rate coefficient depend only on the value of the reduced electric field $E/n$ (where $n$ is the number density of the gas), the electron-neutral collisional processes considered and their respective cross-sections. The Bolsig+ kinetic solver[6] is used as a benchmark solution method against which the different DSMC solutions are compared. All cross-section data used in the present work was sourced from the LXCat database.[22]

We consider two different mixtures: a xenon plasma ($Xe/Xe^+/e^-$) and a helium plasma ($He/He^+/e^-$). Two values of the reduced electric field are used for the simulations: 100 and 750 Td for xenon, and 25 and 100 Td for helium. The initial number density of neutral species is taken to be $10^{23}$ m$^{-3}$, and the initial number density of the electrons is taken as $10^{16}$ m$^{-3}$. A timestep of 50 fs is used for the simulations. The instantaneous ionization rates are computed at each timestep and statistics are gathered once the steady ionizing state has been reached.

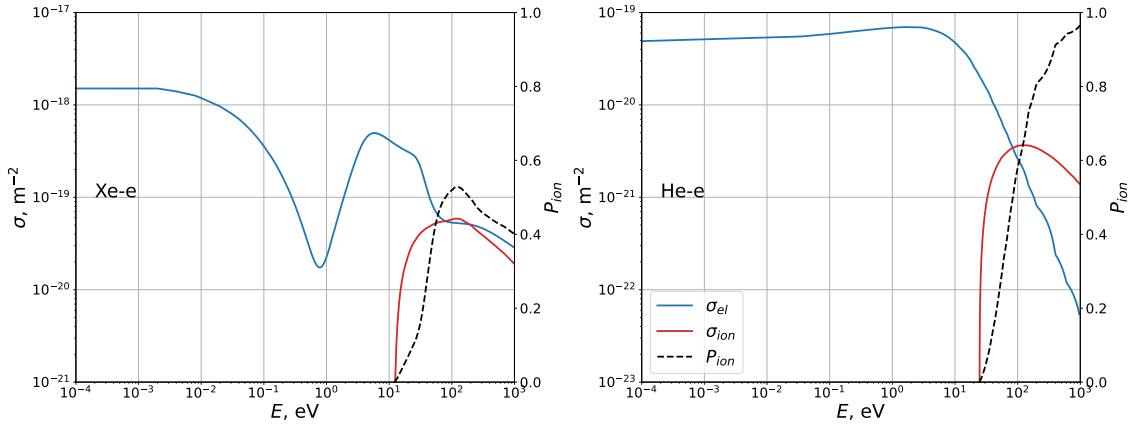


Figure 1: Electron-neutral elastic scattering and ionization cross-sections as a function of the relative translational energy for xenon (left) and helium (right). The dashed line shows the ionization probability as a function of the relative translational energy.

For xenon, the Complex Optical Potential (COP) cross-section data[15,16] is used for the elastic electron-neutral scattering, along with the Hayashi[10] data on ionization cross-sections. The Okhrimovskyy scattering model[21] is used for the anisotropic scattering. For helium, the the elastic and ionization cross-sections were taken from the Biagi dataset,[1] and the electron-neutral scattering was assumed to be isotropic. Figure 1 shows the elastic scattering and ionization cross-sections for electron-neutral collisions, as well as the ionization probability. It can be seen that despite the significantly higher ionization energy of helium, the probability of ionization increases much more rapidly with increasing collisional energy than for xenon. Thus, one might expect that the event splitting scheme will provide more computational benefit for the case of a xenon plasma, as even at high collision energies the ionization probability does not exceed 0.5, whereas in helium, as the energy increases, the ionizaton becomes the dominant collisional process.

In order to compare the different collision schemes, the number of simulation particles was varied from 200 particles to 5000 particles, with the number of neutral and electron particles taken to be equal (for the purposes of this spatially homogeneous slightly ionized test case, the produced ions were discarded, as they have no impact on the simulation). The adaptive octree merging scheme[14] was used for particle merging, with merging applied when the number of particles of a certain species exceeded the specified target number of particles of that species by more than 10%.

Figure 2 shows the rate coefficients computed with the standard DSMC ("sampling") scheme and the event splitting scheme, as well as the variance in the computed values, as a function of the computational time per timestep. The computed values show good agreement with the reference Bolsig+ solution. As the number of simulation particles is increased, the computational time increases as well, and the variance is reduced. Use of the event splitting scheme reduces the variance in the ionization rate coefficient by roughly a factor of 10 for the 100 Td reduced field, and by up to a factor of 3-4 for the 750 Td reduced field. As the noise in DSMC simulations scales as $1/\sqrt{N_p}$ (where $N_p$ is the

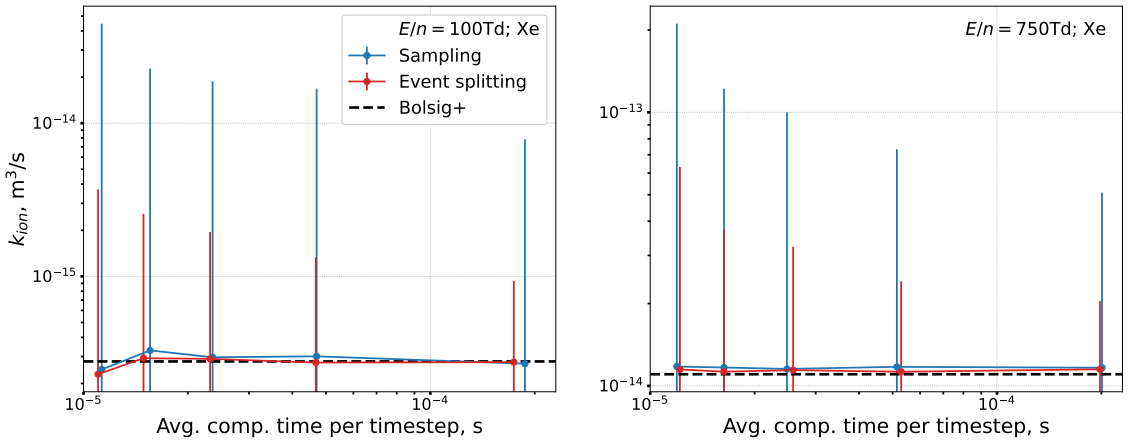


Figure 2: Mean value of the ionization rate coefficient in xenon plotted against the average computational time per timestep for a reduced field of 100 Td (left) and 750 Td (right). Vertical bars denote a range of ±1 standard deviation in the computed value of the ionization rate coefficient.

number of simulation particles), achieving the same level of noise using the standard sampling scheme would require using between 10 and 100 as many particles; and as a consequence, increase the computational time by (at least) a factor of 10 as well.

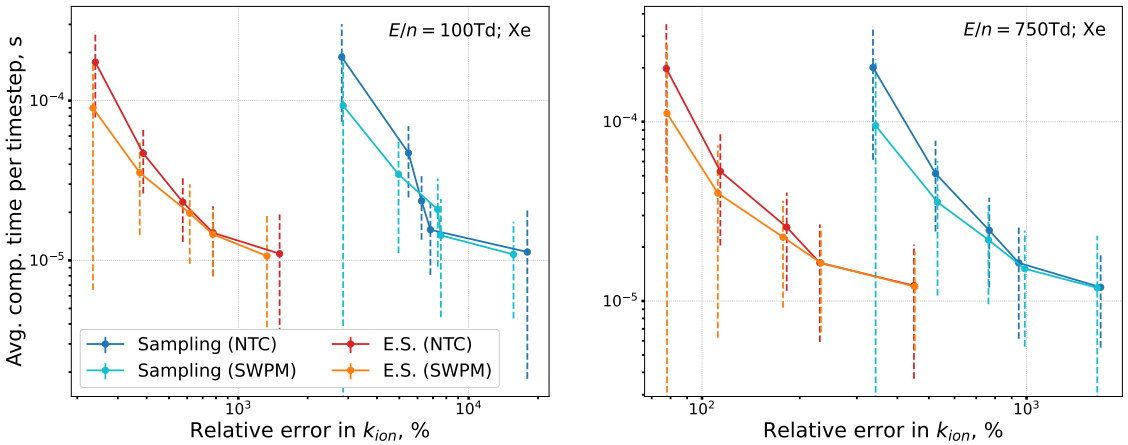


Figure 3: Average computational time per timestep plotted against the relative error in ionization rate coefficient in xenon for a reduced field of 100 Td (left) and 750 Td (right). Vertical bars denote a range of ±1 standard deviation in the average computational time per timestep.

Figure 3 shows the average computational time per timestep plotted against the relative error in the ionization rate coefficient, defined as

$$\mathrm{Err}(k_{ion}) = 100\% \times \frac{1}{\overline{k}_{ion}} \sqrt{\frac{\sum_t \left(k_{ion}^{(t)} - \overline{k}_{ion}\right)^2}{N_t}}, \tag{6}$$

where $N_t$ is the number of timesteps over which the statistics are computed, $k_{ion}^{(t)}$ is the instantaneous ionization rate coefficient at timestep $t$, and $\overline{k}_{ion}$ is the computed mean value of the ionization rate coefficient. From Fig. 3 one can clearly see the significant computational advantage one obtains when the event splitting scheme is used. The difference between the variable-weight NTC and SWPM collision selection schemes is not significant when relatively few particles are used in the simulation; however, as the particle count is increased, the SWPM scheme provides an advantage in terms of computational speed, reducing the required computational time by a factor of 2 when 5000 particles are used for the simulation. A preliminary analysis shows that at higher particle counts, the SWPM scheme computes 20-25% fewer collisions on average at each timestep compared to the NTC scheme. This not only leads to less computational effort spent on the cross-section calculations and simulation of scattering events, but also reduces

the frequency of merging, as fewer particles are produced as a result of the smaller number of collisions.

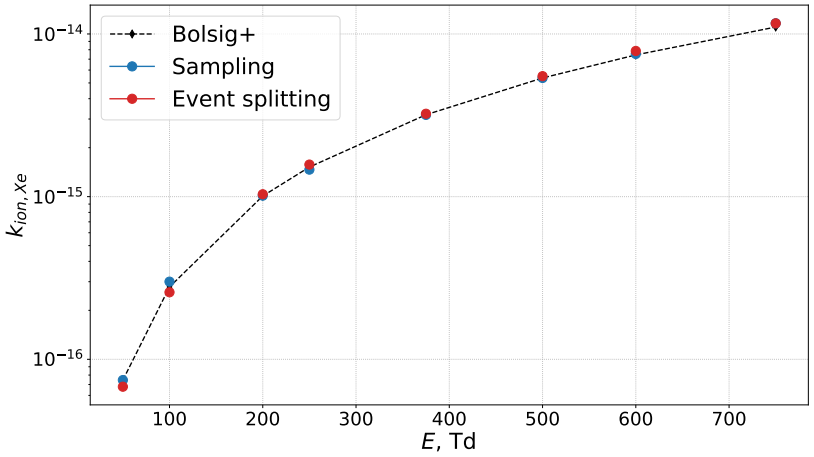


Figure 4: Ionization rate coefficient in xenon computed for different values of the reduced electric field.

Finally, we verify the collision schemes and cross-section implementation for xenon by comparing results with Bolsig+ over a range reduced field values from 50 to 750 Td, as shown on Fig. 4. The results were computed using 2000 particles; overall, a good agreement can be seen between the sampling and event splitting methods and the reference solution throughout the whole range of electric fields considered.

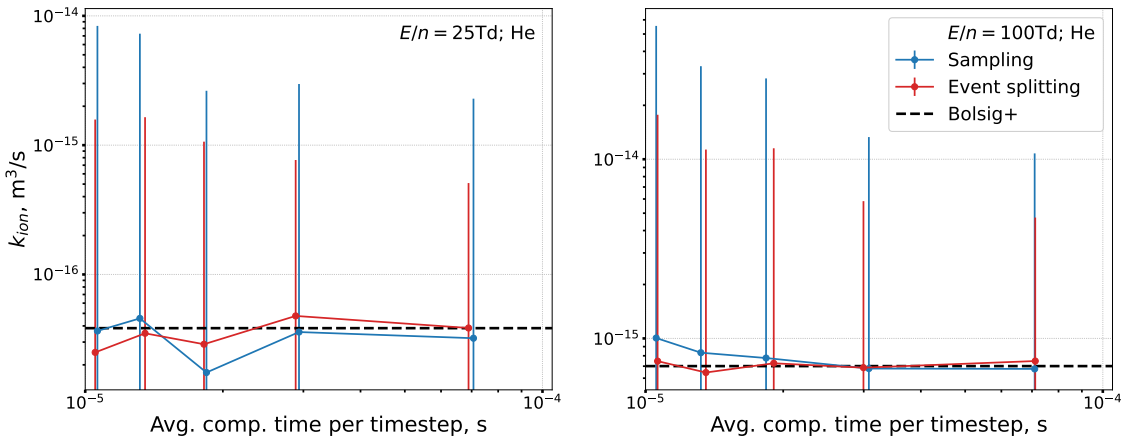


Figure 5: Mean value of the ionization rate coefficient in helium plotted against the average computational time per timestep for a reduced field of 25 Td (left) and 100 Td (right). Vertical bars denote a range of ±1 standard deviation in the computed value of the ionization rate coefficient.

Next, the case of the helium plasma is considered. The Bolsig+ solutions are considered only for reduced field strengths of up to 150 Td, as at higher values of the applied electric field the results may be non-converged, or differences due to the extrapolation schemes used may cause differences compared to the DSMC solutions.[1]

Figure 5 shows the ionization rates plotted against the average computational time per timestep as the number of simulation particles (and, accordingly, the average computational time) is increased. Due to the small collision cross-sections, a much higher level of noise is observed (compared to the case of the xenon plasma); however, the event splitting scheme still performs better than the standard sampling method.

Figure 6 shows the average computational time per timestep plotted against the relative error in the ionization rate coefficient for the helium plasma. As can be seen, there is little difference between the NTC and SWPM collision selection schemes in terms of computational effort; however, some benefit in terms of reduced variance is obtained. Overall, the trend remains the same — as the field strength is increased, the difference in terms of noise between the sampling and event splitting schemes becomes smaller, but the event splitting scheme continues to provide an advantage in terms of level of noise obtained for a given number of particles (or, conversely, the number of particles/computational time per timestep required to achieve a certain level of stochastic noise).

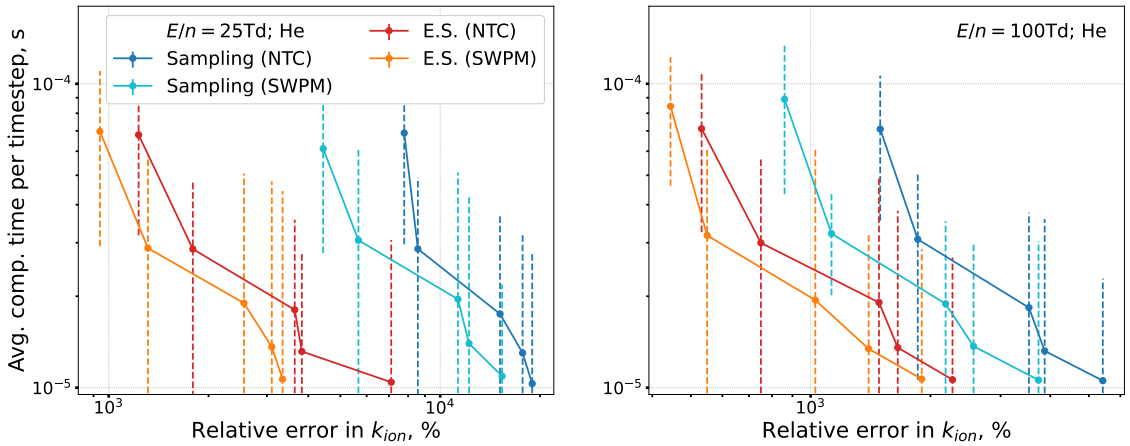


Figure 6: Average computational time per timestep plotted against the relative error in ionization rate coefficient in helium for a reduced field of 25 Td (left) and 100 Td (right). Vertical bars denote a range of ±1 standard deviation in the average computational time per timestep.

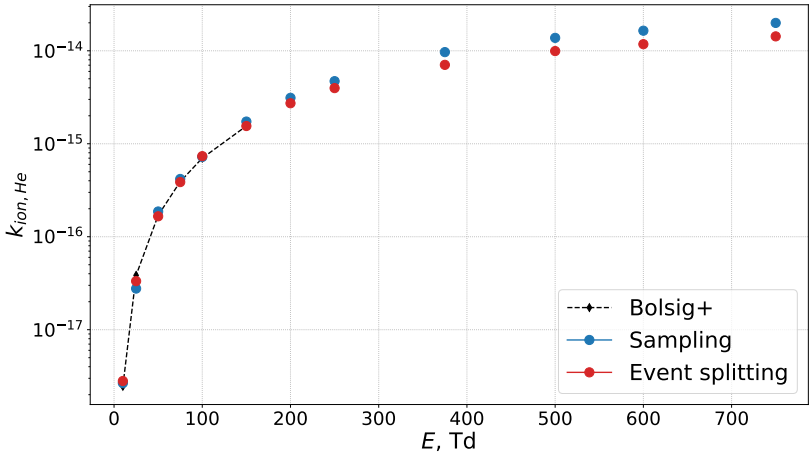


Figure 7: Ionization rate coefficient in helium computed for different values of the reduced electric field, isotropic scattering.

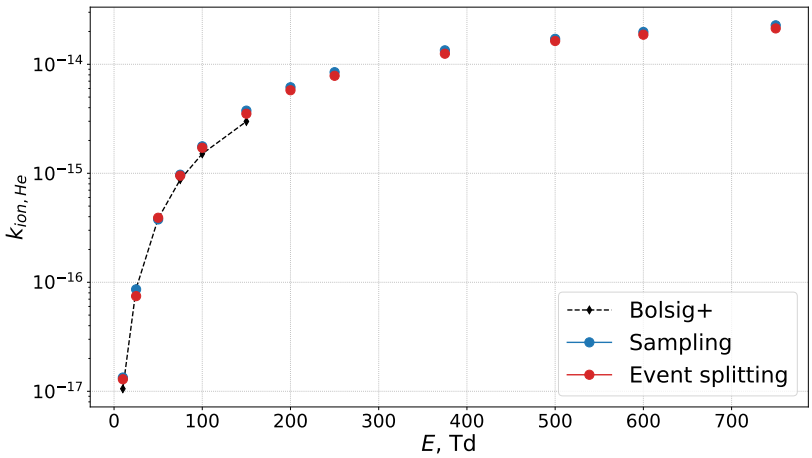


Figure 8: Ionization rate coefficient in helium computed for different values of the reduced electric field, anisotropic scattering.

Figure 7 shows the ionization rate coefficients computed with the sampling and event splitting collision schemes for different values of the reduced field strength, ranging from 10 to 750 Td. We see that as the field strength is increased, the results produced by the two collision schemes begin to diverge. In order to investigate the source of this difference, simulations using the anisotropic scattering model[21] were also performed. The results are shown on Fig. 8, and it can be seen that the two collision methods agree well with each other. A possible reason for the discrepancy between the results obtained with the sampling and event splitting schemes when using isotropic scattering can thus be hypothesized. In helium, at higher electron energies, ionization is the more probable process (as seen from Fig. 1). The standard sampling approach thus may lead to insufficient sampling of scattering events, and underestimate the back-scattering when the isotropic scattering model is used, leading to higher electron energies and an over-estimated ionization rate coefficient. The anisotropic scattering model leads to predominantly forward scattering at higher collision energies;[21] thus, the accurate sampling of back-scattering collisions plays a lesser role. A more detailed study of the role of event splitting when sampling anisotropic scattering is planned for future work. The current results show the benefit from the improved sampling of uncommon events that the event splitting scheme provides.

### 3.2 1-D RF Plasma Simulation

Next, we consider a one-dimensional capacitively coupled RF plasma simulation in helium. The conditions were based on the second benchmark test case of Turner et al.[28] A 13.56 MHz RF source of 200 V was assumed, and a timestep of 1/800 $\tau$ (where $\tau$ is the RF source period) was used. The neutral density was taken to be $32.1 \times 10^{20}$ m$^{-3}$, and the density of ions and electrons at $t = 0$ was taken to be $5.12 \times 10^{14}$ m$^{-3}$. The domain width was taken to be 6.7 cm, and 256 cells were used for the discretization. No secondary emission from the walls is assumed. In the present work, the ion-elastic collisions and electron-impact excitation reactions were not taken into account. First-order shape functions were used for the charge deposition and electric field interpolation, and the tridiagonal matrix algorithm was used to solve the Poisson equation. The particle advection was performed using the Velocity Verlet algorithm and the variable-weight NTC collision scheme was used. The average number of particles per cell was varied from approximately 55 particles/cell to 550 particles/cell. All macroscopic quantities were RF cycle-averaged.

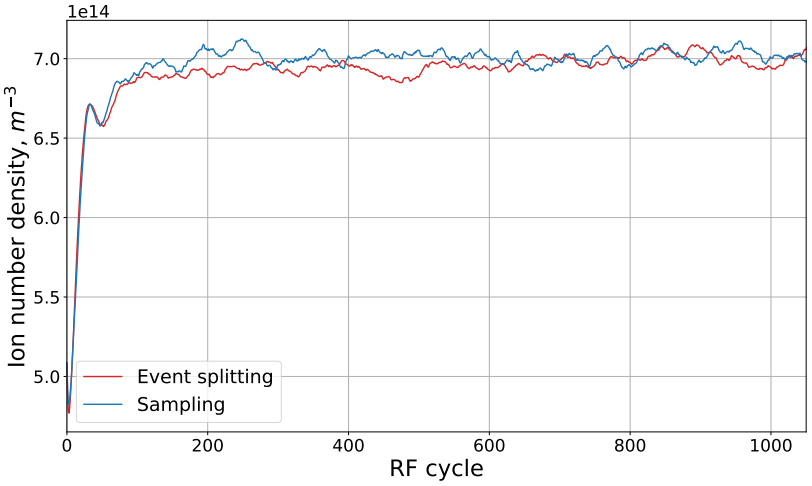


Figure 9: Spatially and cycle-averaged ion number density plotted against the RF cycle number.

Figure 9 shows the spatially and cycle-averaged ion number density as a function of the RF cycle number for the simulations that used 550 particles/cell. It can be seen that both collision methods converge to the same ion number density of approximately $7{\times}10^{14}$ m$^{-3}$, which is comparable to the benchmark value of $8.28{\times}10^{14}$ m$^{-3}$.[28] As the present simulations did not include ion-neutral collisions and electron-impact excitation reactions, a direct comparison is not possible.

In order to evaluate the performance of the collision schemes, we consider the noise in the cycle-averaged ionization rate coefficient (averaging was started at the $200^{th}$ cycle and carried out over 1000 RF cycles). Figure 10 shows the temporal mean of the electron-impact ionization rate coefficient throughout the simulation domain, as well as the region between the $5^{th}$ and $95^{th}$ percentiles (computed over the averaging period) when 550 particles/cell are used for the simulation. One can see that while the mean values produced by the sampling and event splitting schemes are in good agreement, the sampling approach to collisional process type selection leads to a significantly higher level of noise. To compare the event splitting and sampling approaches in more detail, we first calculate the relative level of

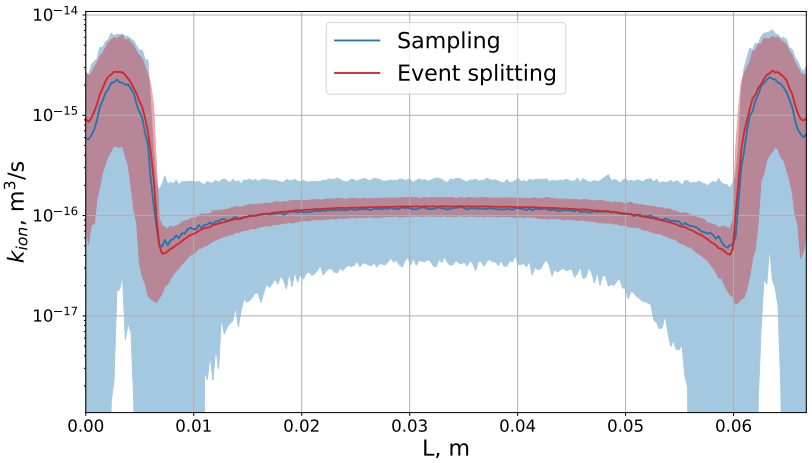


Figure 10: Time-averaged value of the ionization rate coefficient (solid lines) and the range between the $5^{th}$ and $95^{th}$ percentiles (shaded regions) plotted throughout the simulation domain

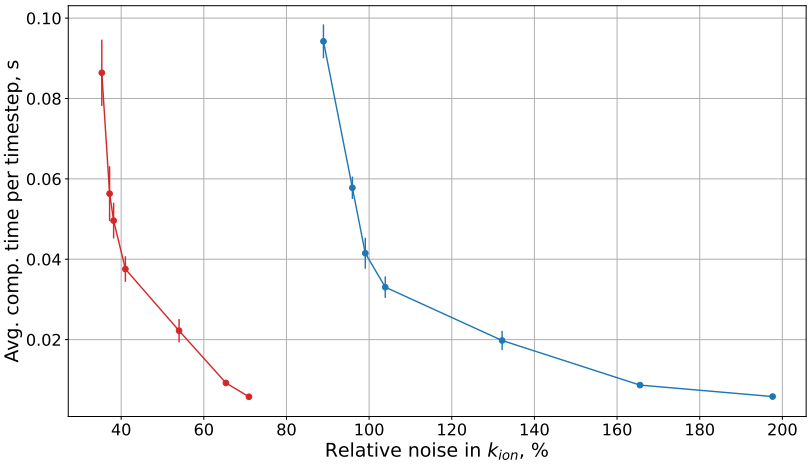


Figure 11: Average computational time per time-step plotted against the relative error in the ionization rate coefficient.

noise in the ionization rate coefficient at each spatial location by computing the standard deviation and dividing it by the mean value of the ionization rate coefficient at that location. Next, we average the relative level of noise throughout the domain and plot the computational effort against this relative noise, as shown on Fig. 11. Use of the event splitting scheme allows for a 2.5-fold reduction in noise in the ionization rate coefficient for the same level of computational cost.

## 4. Conclusions

The modelling of collisions and inelastic processes in particular in PIC-DSMC simulations is studied for xenon and helium plasmas. It is shown that the use of the recently developed event splitting scheme provides significant benefit for the accuracy of ionization rate modelling in xenon: achieving similar levels of stochastic noise with the standard DSMC sampling procedures requires from one to two orders of magnitude more particles and computational time. Furthermore, use of the SWPM collision scheme can provide benefits in terms of computational expense and/or stochastic noise reduction. In helium, at high applied field strengths, use of the event splitting scheme may improve the simulation of rare elastic back-scattering events.

In a 1-D RF plasma simulation in helium, use of the event splitting scheme provides a noticeable reduction in the level of stochastic noise in the ionization rate coefficient.

Further extensions of the collision scheme are planned to include charge-exchange (CEX) collisions and excitation processes.

## 5. Acknowledgments

This work was supported in part by Sandia National Laboratories. Sandia National Laboratories is a multimission laboratory managed and operated by National Technology and Engineering Solutions of Sandia, LLC., a wholly owned subsidiary of Honeywell International, Inc., for the U.S. Department of Energy's National Nuclear Security Administration under contract DE-NA0003525. This paper describes objective technical results and analysis. Any subjective views or opinions that might be expressed in the paper do not necessarily represent the views of the U.S. Department of Energy or the United States Government. SAND2022-7773 C

Georgii Oblapenko acknowledges the funding provided by the Alexander von Humboldt foundation for his stay as a guest researcher at the German Aerospace Center (DLR).

## References

[1] Alves, L., K. Bartschat, S. Biagi, M. Bordage, L. Pitchford, C. Ferreira, G. Hagelaar, W. Morgan, S. Pancheshnyi, A. Phelps, et al. 2013. Comparisons of sets of electron–neutral scattering cross sections and swarm parameters in noble gases: II. Helium and neon. *J. Phys. D: Appl. Phys.*, 46(33):334002.

[2] Araki, S., and R. Martin. 2020. Interspecies fractional collisions. *Phys. Plasmas*, 27(3):033504.

[3] Boyd, I. 1996. Conservative species weighting scheme for the direct simulation Monte Carlo method. *J. Thermophys. Heat Transfer*, 10(4):579–585.

[4] Boyd, I. 2001. Review of Hall thruster plume modeling. *J. Spacecr. Rockets*, 38(3):381–387.

[5] Celik., M., M. Santi, S. Cheng, M. Martinez-Sanchez, and J. Peraire. 2003. Hybrid-PIC simulation of a Hall thruster plume on an unstructured grid with DSMC collisions. In *28th International Electric Propulsion Conference, Toulouse, France*, pages 1–10.

[6] Hagelaar, G., and L. Pitchford. 2005. Solving the Boltzmann equation to obtain electron transport coefficients and rate coefficients for fluid models. *Plasma Sources Sci. Technol.*, 14(4):722.

[7] Hara, K. 2019. An overview of discharge plasma modeling for Hall effect thrusters. *Plasma Sources Sci. Technol.*, 28(4):044001.

[8] Hara, K., M. Sekerak, I. Boyd, and A. Gallimore. 2014. Mode transition of a Hall thruster discharge plasma. *J. Appl. Phys.*, 115(20):203304.

[9] Hara, K., M. Sekerak, I. Boyd, and A. Gallimore. 2014. Perturbation analysis of ionization oscillations in Hall effect thrusters. *Phys. Plasmas*, 21(12):122103.

[10] Hayashi, M. 2003. Bibliography of electron and photon cross sections with atoms and molecules published in the 20th century. Xenon. Technical report, National Inst. for Fusion Science.

[11] Holste, K., P. Dietz, S. Scharmann, K. Keil, T. Henning, D. Zschätzsch, M. Reitemeyer, B. Nauschütt, F. Kiefer, F. Kunze, et al. 2020. Ion thrusters for electric propulsion: Scientific issues developing a niche technology into a game changer. *Rev. Sci. Instrum.*, 91(6):061101.

[12] Lama, S., J. Zweck, and M. Goeckner. 2020. A higher order moment preserving reduction scheme for the Stochastic Weighted Particle Method. *SIAM J. Sci. Comp.*, 42(5):A2889–A2909.

[13] Lapenta, G., and J. Brackbill. 1994. Dynamic and selective control of the number of particles in kinetic plasma simulations. *J. Comput. Phys.*, 115(1):213–227.

[14] Martin, R., and J. Cambier. 2016. Octree particle management for DSMC and PIC simulations. *J. Comput. Phys.*, 327:943–966.

[15] McEachran, R. and A. Stauffer. 2015. Viscosity cross sections for the heavy noble gases. *Eur. Phys. J. D*, 69(4):1–4.

[16] McEachran, R. and A. Stauffer. 2014. Momentum transfer cross sections for the heavy noble gases. *Eur. Phys. J. D*, 68(6):1–8.

[17] Moore, C., S. Moore, M. Hopkins, J. Boerner, K. Cartwright, and L. Biedermann. 2015. Timestep constraints for accurate PIC-DSMC simulation of breakdown: From arc initiation to stable arcs. Technical report, Sandia National Lab.(SNL-NM), Albuquerque, NM (United States).

[18] Nuwal, N., R. Jambunathan, and D. Levin. 2020. Kinetic modeling of spacecraft surfaces in a plume backflow region. *IEEE Trans. Plasma Sci.*, 48(12):4305–4325.

[19] Oblapenko, G., D. Goldstein, P. Varghese, and C. Moore. 2021. Hedging Direct Simulation Monte Carlo bets via event splitting. *accepted in J. Comput. Phys.*.

[20] Oblapenko, G., D. Goldstein, P. Varghese, and C. Moore. 2022. Improving PIC-DSMC simulations of electrical breakdown via event splitting. In *AIAA Scitech 2022 Forum*, paper 215.

[21] Okhrimovskyy, A., A. Bogaerts, and R. Gijbels. 2002. Electron anisotropic scattering in gases: A formula for Monte Carlo simulations. *Phys. Rev. E*, 65(3):037402.

[22] Pitchford, L., L. Alves, K. Bartschat, S. Biagi, M. Bordage, I. Bray, C. Brion, M. Brunger, L. Campbell, A. Chachereau, et al. 2017. Lxcat: An open-access, web-based platform for data needed for modeling low temperature plasmas. *Plasma Processes Polym.*, 14(1-2):1600098.

[23] Rjasanow, S. and W. Wagner. 1996. A stochastic weighted particle method for the Boltzmann equation. *J. Comput. Phys.*, 124(2):243–253.

[24] Romano, F., J. Espinosa-Orozco, M. Pfeiffer, G. Herdrich, N. Crisp, P. Roberts, B. Holmes, S. Edmondson, S. Haigh, S. Livadiotti, et al. 2021. Intake design for an atmosphere-breathing electric propulsion system (ABEP). *Acta Astronautica*, 187:225–235.

[25] Schmidt, D., and C. Rutland. 2000. A new droplet collision algorithm. *J. Comput. Phys.*, 164(1):62–80.

[26] Serikov, V., S. Kawamoto, and K. Nanbu. 1999. Particle-in-cell plus direct simulation Monte Carlo (PIC-DSMC) approach for self-consistent plasma-gas simulations. *IEEE Trans. Plasma Sci.*, 27(5):1389–1398.

[27] Sun, A., M. Becker, and D. Loffhagen. 2016. PIC/MCC simulation of capacitively coupled discharges: Effect of particle management and integration. *Comput. Phys. Commun.*, 206:35–44.

[28] Turner, M., A. Derzsi, Z. Donko, D. Eremin, S. Kelly, T. Lafleur, and T. Mussenbrock. 2013. Simulation benchmarks for low-pressure plasmas: Capacitive discharges. *Phys. Plasmas*, 20(1):013507.